Int. J. Electrochem. Sci., 16 **(2021)** Article ID: 210942, doi: 10.20964/2021.09.18

International Journal of
ELECTROCHEMICAL
SCIENCE
www.electrochemsci.org

Electrodeposition of well-crystalline Ni-Co alloy thin films on steel substrates from aqueous solutions containing citrate anions

M. M. Kamel[1,*], *E. Alzahrani*[2], *I. S. Ibrahim*[3], *S. M. Rashwan*[1]

[1] Department of Chemistry, Faculty of Science, Suez Canal University, Ismailia, 41522 Egypt
[2] Department of Chemistry, College of Sciences, Taif University, P.O. Box 11099, Taif 21944, Saudi Arabia.
[3] General Organization for Exports and Imports Control (GOEIC), (RIIL), Sokhna Port, Suez, Egypt.
[*]E-mail: medhat_darwish@science.suez.edu.eg

Received: 2 May 2021 / *Accepted:* 27 June 2021 / *Published:* 10 August 2021

The electrochemical deposition of Ni-Co alloy thin films onto steel coupons was carried out from aqueous solutions containing citrate anion under various operating conditions. The deposition process was investigated from a bath containing $NiSO_4.6H_2O$, $CoSO_4.7H_2O$, $Na_3C_6H_5O_7.2H_2O$, and Na_2SO_4. The impact of bath constituents, applied current, and temperature on current efficacy (CCE) and composition of the alloy was investigated. The plating of the alloy belongs to the regular type, in which the nobler metal (Ni) is preferably deposited. The CCE is very high and rises with a rising $[Ni^{2+}]$ / $[Co^{2+}]$ ratio in the bath and stirring speed of the plating solution. However, it tends to decrease as the current density, temperature, or concentration of citrate ions increases. The quantity of Co metal in the plated alloy is ameliorated with increasing stirring speed, temperature, and Co^{2+} ions concentration. The appearance and the crystal texture of the coatings were checked by electron microscope and X-ray diffraction tools. The deposits obtained from the given bath are well-crystalline and have an (FCC) structure. The throwing power and throwing index of the tub are estimated and revealed that the alkaline citrate tub has good throwing power.

Keywords: Electrodeposition; Citrate anions; Steel coupons; Ni-Co; Alloy; Thin films

1. INTRODUCTION

An alloy is a substance that has metallic properties and consists of two or more chemical elements of which at least one element is a metal. Alloys oftentimes possess properties that are different from the metals they contain. This makes them more valuable than their parent metals alone.

Among various alloys, electrodeposited Ni-Co alloy has found great interest for several years. This is mainly due to their versatility, lightweight, brightness, smooth surface, ductility, low-temperature superplasticity, high thermal stability, excellent magnetic properties, and high heat

conductivity. In addition to electrocatalytic activity, high strength even at elevated temperatures, low stress, high hardness, good adhesion to the substrate, good chemical stability, and superior wear, abrasion, and corrosion resistance at elevated temperatures [1 – 3]. Accordingly, electrodeposited Ni-Co coatings are important engineering materials, widely utilized as decorative and protective coatings in hard environments comprising water or corrosive materials that may cause significant wear and oxide scaling at high temperatures and in several industrial fields such as automobile, aerospace, rocket technology, cosmonautics and electronics [4, 5]. In addition to this and because of their electrocatalytic activity, electrodeposited Ni-Co alloys are utilized as active components for the hydrogen and oxygen evolution reactions in water electrolysis [6].

Due to their superior properties and advanced applications, many researchers extensively studied Ni-Co alloy coatings [7-15]. Lupi et al. [7] studied the electrocatalytic performance of nickel-cobalt alloy cathodes for H_2 evolution in alkaline media. Ni-Co alloy with varying cobalt amounts was electrodeposited from sulfamate tub by Srivastava and others [8]. Furthermore, Ma et al. [5] electrodeposited nanocrystalline Ni-Co coatings with different cobalt quantities. Hassani and his colleagues [4] electrodeposited nanocrystalline Ni-Co coatings from a modified Watts bath. Karpuz et al. [9] studied the properties of the electroplated Ni-Co alloy obtained from electrolytes containing nickel sulfamate, cobalt sulfate, and boric acid. Also, Olvera et al. [10] studied the structural properties of electrodeposited Co_xNi_{100-x}. The development and optimization of electroplated Co-Ni alloys for biomedical microdevices applications were performed by Ergeneman et al. [11].

The electrodeposition of Ni-Co alloys from the majority of baths pertains to anomalous kind [16]. The less noble Co metal preferably deposits at the expense of the nobler Ni. The operating parameters like current density, bath temperature, utilization of organic components, the concentration of solution constituents results in an amendment in the kinetics of the deposition process, the structure, and appearance of the deposits.

The electroplating processes are mainly investigated from tubs comprising ligands. Different ligands like lactates, tartrates, sulfamates, citrates, and gluconates have been utilized. These ligands are safe, easily got and their disintegration products offering simple handling [17-26].

The present work aims to fabricate crystalline Ni-Co alloy thin films onto steel substrate from alkaline citrate bath by electrodeposition technique under various operating conditions like the composition of the bath, the applied current density, pH, agitation speed, temperature, and deposition time. In addition, this investigation studied the impact of these parameters on the polarization, cathodic efficacy, throwing power (TP), throwing index (TI), and the composition of the deposits. The morphology and crystal structure of the deposits were also tested.

2. EXPERIMENTAL PROCEDURE

The practical experiments were established from baths with compositions: 0.08 – 0.19 M $NiSO_4.6H_2O$, 0.01 - 0.12 M $CoSO_4.7H_2O$, 0.3 – 1.0 M $Na_3C_6H_5O_7.2H_2O$, and 0.2 M Na_2SO_4. The overall concentration of metal sulfates was preserved constantly at 0.20 M. The solutions were

prepared immediately before starting the experiments, using bi-distilled water and fine chemicals. The pH was controlled by NH_4OH and was determined by a Fisher device.

The electrodeposition cell was depicted formerly [27]. It made from a Perspex trough, equipped with a steel cathode and stainless steel (type 304) anode. Both the two electrodes had 3 × 3 cm dimensions. The negative electrode was abrasive with polishing paper. Then it washed with bi-distilled water, ethyl alcohol, and finally weighed. The plating process was achieved from agitated solutions. The plating duration was 20 minutes, after which the substrate was taken away, washed with bi-distilled water, exsiccated, and weighed.

The alloy compositions are identified with the help of an atomic absorption spectrometer (Thermo, model; SOLAAR), after dissolving the coatings in 32% hydrochloric acid and diluting with bi-distilled water. The cathodic current efficacy for the alloy deposition, CCE, equals the sum of the cathodic current efficacies of the parent metals.

$$CCE = CCE_{Ni} + CCE_{Co} \quad (1)$$

The % of cobalt metal in the alloy was estimated by the following relation:-

$$Co_{(alloy)}\% = [(\text{mass of } Co_{(alloy)}) / (\text{mass of } Co_{(alloy)} + \text{mass of } Ni_{(alloy)})] \times 100 \quad (2)$$

The % of cobalt metal in the bath is determined using the following relation [28]:-

$$Co_{(bath)}\% = [(\text{mass of } Co_{(bath)}) / (\text{mass of } Co_{(bath)} + \text{mass of } Ni_{(bath)})] \times 100 \quad (3)$$

The polarization measurements were carried out in the traditional glass cell, where the working electrode was a steel desk with an area of 0.785 cm^2. The counter electrode was Pt gauze and the reference electrode was Calomel (SCE). The electrodes were connected to a potentiostat /galvanostat, model 273 controlled by a computer. All the experiments were carried out at a scan rate of 20 mV s^{-1}.

The throwing power & the throwing index of the bath were determined via a circuit previously described [16]. The plating cell was made from a Perspex trough with the inside dimensions of 20 × 3 × 2.5 cm. The cell was provided with one stainless steel anode between two parallel cathodes at different distance ratios (1:1 – 1:3). The throwing power was computed by Field's equation [28]:-

$$TP\% = \frac{L\text{-}M}{L+M\text{-}2} \times 100 \quad (4)$$

Where L is the linear ratio (L = 1, 2, or 3), and M is the metal distribution ratio (m_{near} / m_{far}). The magnitudes of M were recorded as a function of L over a range of linear ratios varying between 1:1 and1:3. By plotting L (X-axis) versus M (Y-axis), we get a straight line. The reciprocal of the straight line is known as the throwing index. It is an immediate measure for the bath throwing power.

The appearance of the electroplated alloy was examined by scanning SEM (QUANTA FEG 250). The phase and crystal structure of the coating was studied by X-ray instrument (X`pert Pro P analytical, operated at 45 kV and 40 mA with Cu-K_α, λ = 1.540 ^oA).

3. RESULTS AND DISCUSSION

3.1 Polarization measurements

For this measurement, the potential of the working electrode is changed and the resultant current is recorded versus the applied potential [29]. Cathodic polarization curves can aid in

interpreting the characteristics of the electroplating process. Polarization can affect the CCE, the TP of the baths, and the quality of the electrodeposits [30, 31].

The polarization outlines for the plating of Ni-Co alloy over steel metal under various practical conditions are illustrated in Figs. 1-5. The interrelationship between the measured current density and the applied cathodic potentials for the deposition of Ni, Co, and Ni-Co alloy beneath identical situations is illustrated in Fig. (1). The figure depicts that the deposition of the parent metals, Ni and Co is associated with a considerable overvoltage. Polarization always increases in complex electrolytes. Consequently, further excess energy is required to subdue the barrier of heterogeneous plating over a foreign substrate. The deposition doesn't start till the applied potential attains – 0.62 V for Co^{2+}, – 0.66 V for Ni^{2+}, and – 0.7 V for Ni-Co alloy [31].

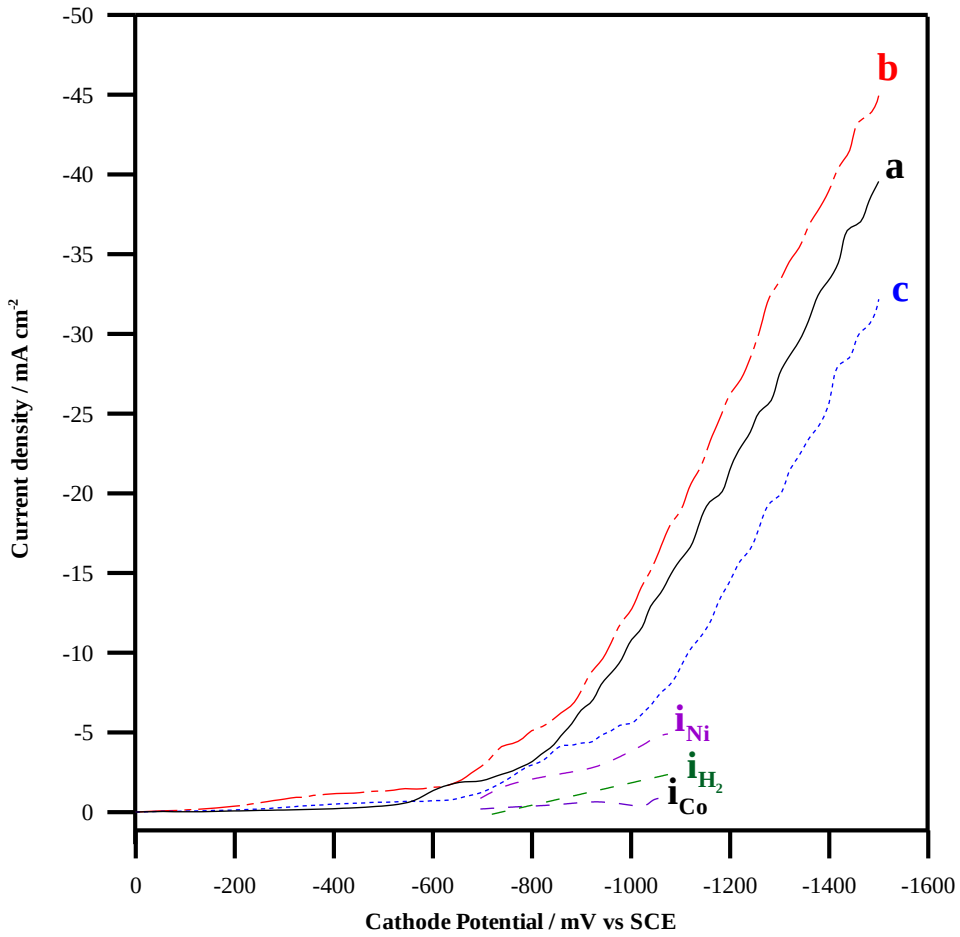

Figure 1. Cathodic polarization curves of (a) nickel from a solution containing 0.08 M $NiSO_4$. $6H_2O$, (b) cobalt from a solution containing 0.12 M $CoSO_4$. $5H_2O$ and (c) Ni-Co alloy from a solution containing 0.08 M $NiSO_4$. $7H_2O$, 0.12 M $CuSO_4$. $5H_2O$. (- - - -) partial current densities of Ni, Co, and H_2 during the electrodeposition of Ni-Co alloy. Scan rate = 20 mV/s.

The Co polarization curve exists at a more positive potential than Ni. This implies that Co is the nobler one in the given system. The Ni-Co alloy curve locates at highly negative potentials than the individual metals. This behavior can be assigned to some kinetic factors [16]. The obtained data expect

that in the present system, Co would be deposited at the expense of Ni. This expectation is not valid with our experimental results.

The formation of nickel/cobalt citrate complexes depends on their molar ratio. For the given conditions, citrate ions form (1:1) soluble complexes with both Ni^{2+} and Co^{2+}, as the metal ions concentration is low in the light of citrate concentration. i.e., there will be no free Ni^{2+} and Co^{2+} ions in the plating solution [32].

Nickel exists as $[Ni\text{-}Cit]^-$ complex (pK_f = 5.11). Cobalt is present as $[Co\text{-}Cit]^-$ complex (pK_f = 4.83) [33 – 35].

$$Ni^{2+} + Cit^{3-} \leftrightarrows [Ni\text{-}Cit]^- \quad (pK_f = 5.11) \quad (5)$$

$$Co^{2+} + Cit^{3-} \leftrightarrows [Co\text{-}Cit]^- \quad (pK_f = 4.83) \quad (6)$$

As Ni^{2+} and Co^{2+} exist in the plating bath as citrate complexes, the following electro-reduction reactions are therefore applicable, accompanied by simultaneous hydrogen evolution reaction [36 – 38].

$$[Ni\text{-}Cit]^- + 2e^- \leftrightarrows Ni_{(s)} + Cit^{3-} \quad (7)$$

$$[Co\text{-}Cit]^- + 2e^- \leftrightarrows Co_{(s)} + Cit^{3-} \quad (8)$$

Based on the electrochemical deposition experiments, the partial polarization curves for parent metals, Co & Ni, were obtained by estimating the fruitful currents densities used for cobalt and nickel deposition ($\mathbf{i}_{Co}$ and $\mathbf{i}_{Ni}$) from the element contents in the alloy coating and the current efficacy. In any case, the partial currents were interrelated with the corresponding potential response of the total applied current density. The partial current density for hydrogen ($\mathbf{i}_H$) was estimated by subtracting the summation of $\mathbf{i}_{Co}$ & $\mathbf{i}_{Ni}$ from the applied current density. The calculated partial current densities are listed in Table 1.

The partial current density (i_p) of cobalt and Ni metals through the deposition process is a function of their deposition rates. It can be estimated from the composition of the deposit (w), the plating period (t), the mass of coating (m), and the electrochemical equivalent (e) [39].

$$i_p = \frac{m\,w}{100\,e\,t} \quad (9)$$

The i_p of hydrogen gas is obtained with the help of this equation:

$$i_p\,(H_2) = i_{applied} - [(i_p\,(Co) + i_p\,(Ni)] \quad (10)$$

Where $i_{applied}$ is the total applied current density and i_p (Co), i_p (Ni) are the partial current densities of Co and Ni, respectively.

The dotted lines enclosed in Fig. (1) demonstrate the i_p of Ni, Co, and H_2 in the deposition process. The deposition rate of Co is the smallest among other species, Ni and hydrogen. This indicates that the prepared alloy has low cobalt content. The plating of Ni-Co alloy from the given bath satisfies a regular type as the percent of the Co, the more active metal, in the deposit is smaller than its percent in the plating bath [16, 39].

Table 1. Calculated partial current densities of Ni, Co, and H_2 during the deposition process

Current density (mA cm^{-2})	**Potential** (mV/ SCE)	**Partial current densities (mA cm^{-2})**		
		i_{Ni}	**i_{Co}**	**i_{H2}**
1.11	-695	0.865	0.199	0.046
2.22	-749	1.673	0.304	0.244
3.33	-851	2.377	0.482	0.473
4.44	-931	2.878	0.650	0.915
5.56	-996	3.776	0.453	1.325
6.67	-1032	4.381	0.488	1.797
7.78	-1043	4.593	0.731	2.452
8.89	-1074	4.909	0.871	3.107

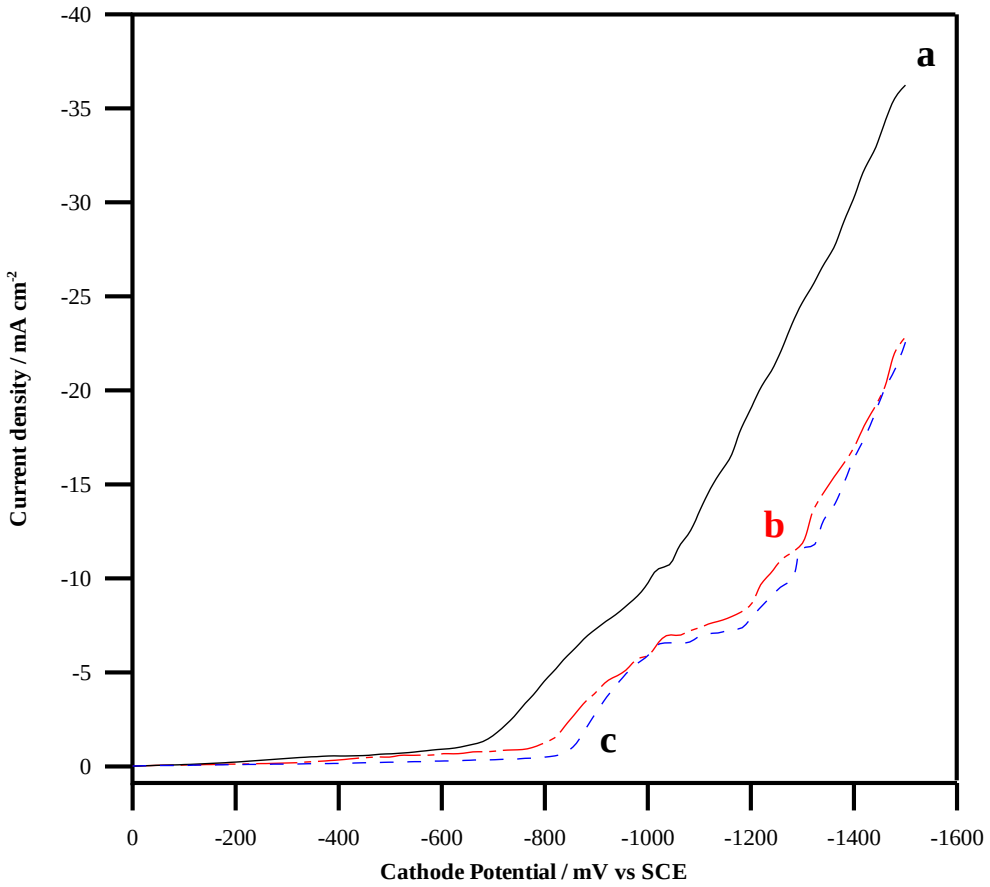

Figure 2. Cathodic polarization curves for the deposition of Ni-Co alloy on steel from solutions with different molar ratios of $[Ni^{2+}]$ / $[Co^{2+}]$: (a) 4, (b) 1, and (c) 0.66. Scan rate = 20 mV/s.

Fig. (2) illustrates the impact of $[Ni^{2+}]$ / $[Co^{2+}]$ molar ratio on the overvoltage of Ni-Co alloy deposition. The polarization curves shift to more negative values as the $[Ni^{2+}]$ / $[Co^{2+}]$ ratio decreases in the bath. As the molar ratio decreases, the concentration of Co^{2+} ions increases in the bath. Rising the Co^{2+} ions concentration tends to decrease the cathodic polarization due to an elevation in the amount of Co^{2+} ions in the diffusion layer [16].

The effect of citrate concentration on the polarization of alloy deposition is shown in Fig. (3). Increasing the citrate quantity in the bath greatly moves the plating potential of the alloy to high positive values. This shift could be attributed to the fact that the addition of citrate ions enhances the deposition of Ni-Co alloy. Moreover, the addition of citrate ions is known to encourage the deposition of Ni via complexation and formation of a homogenous catalyst. Similar results are obtained by Abd El Rehim et al. [37, 38]. Moreover, the citrate ion can act as a facilitator for Ni-Co alloy discharge over the steel cathode and doesn't prohibit the active locations on the steel surface for alloy reduction [40].

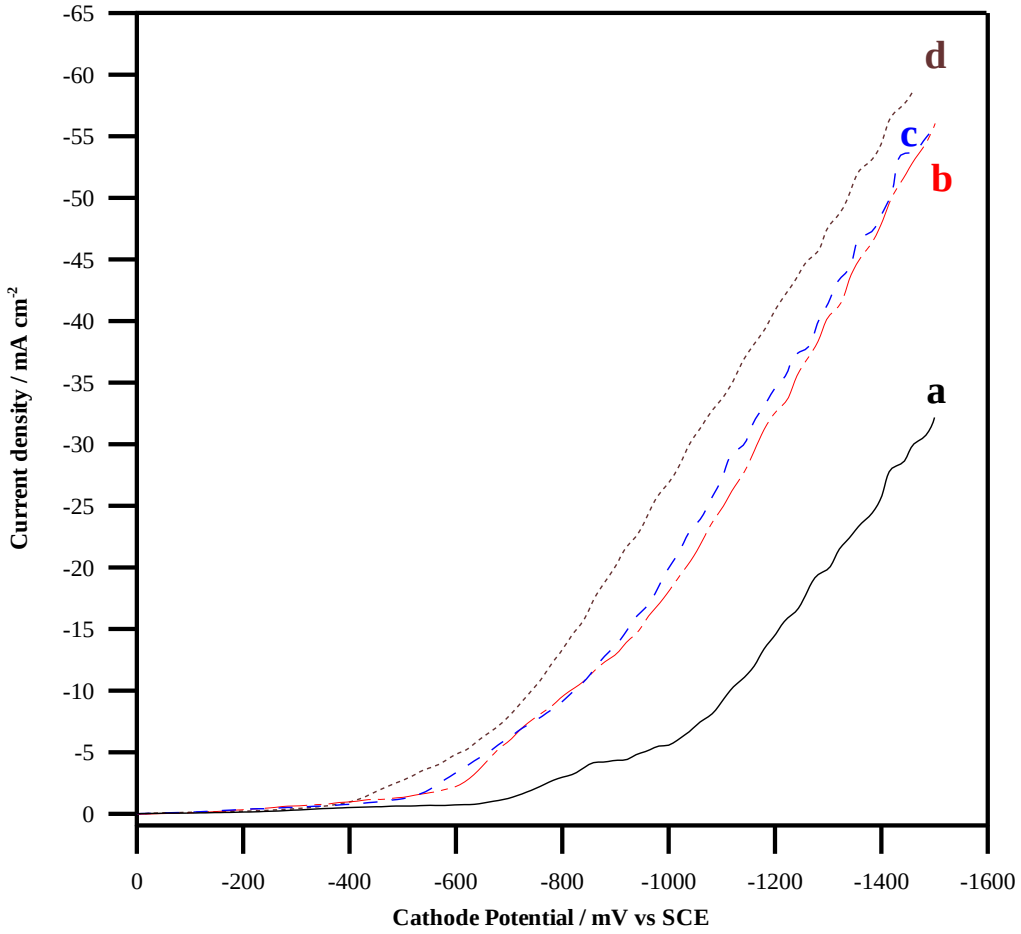

Figure 3. Cathodic polarization curves for the deposition of Ni-Co alloy on steel from solutions containing different concentrations of $Na_3C_6H_5O_7$. $2H_2O$: (a) 0.3, (b) 0.5, (c) 0.8, and (d) 1 M. Scan rate = 20 mV/s.

Fig. (4) illustrates the impact of rising temperature on the polarization of Ni-Co alloy. Raising the bath from 25 to 65°C facilitates the plating of alloy. This is mainly ascribed to suppress the charge-transfer polarization for reducible species. Besides that increasing temperature results in acceleration in the speed of diffusion of the reducing species towards the cathodic diffusion layer. This decreases the concentration type of polarization [31, 35].

Fig. (5) reveals the impact of agitation rate on the of Ni-Co alloy polarization. The polarization curves move toward a noble direction as the agitation speed increases. Increasing agitation speed

enhances the mass transfer of reducible species, and therefore, decreases the thickness of both the concentration and hydrodynamic boundary layers [41].

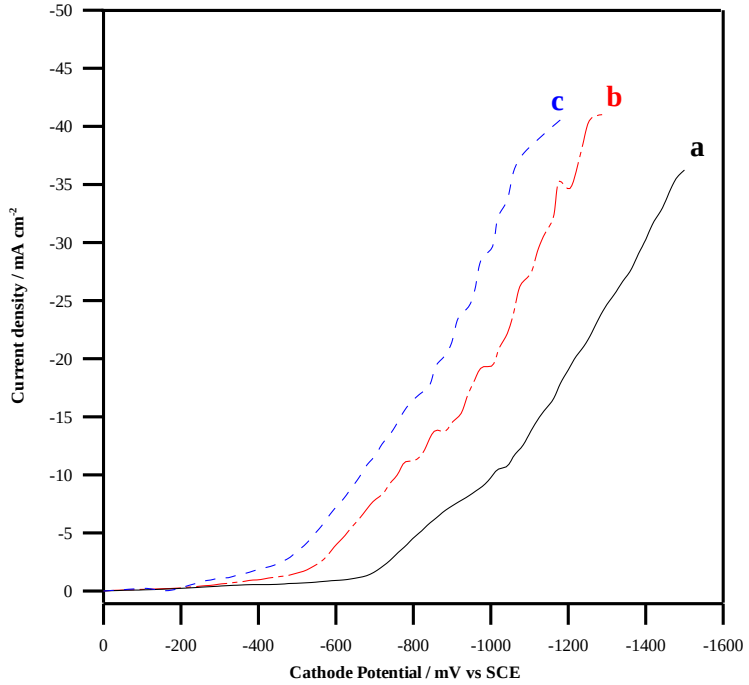

Figure 4. Cathodic polarization curves for the deposition of Ni-Co alloy on steel at different temperatures: (a) 25, (b) 45, and (c) 65 °C. Scan rate = 20 mV/s.

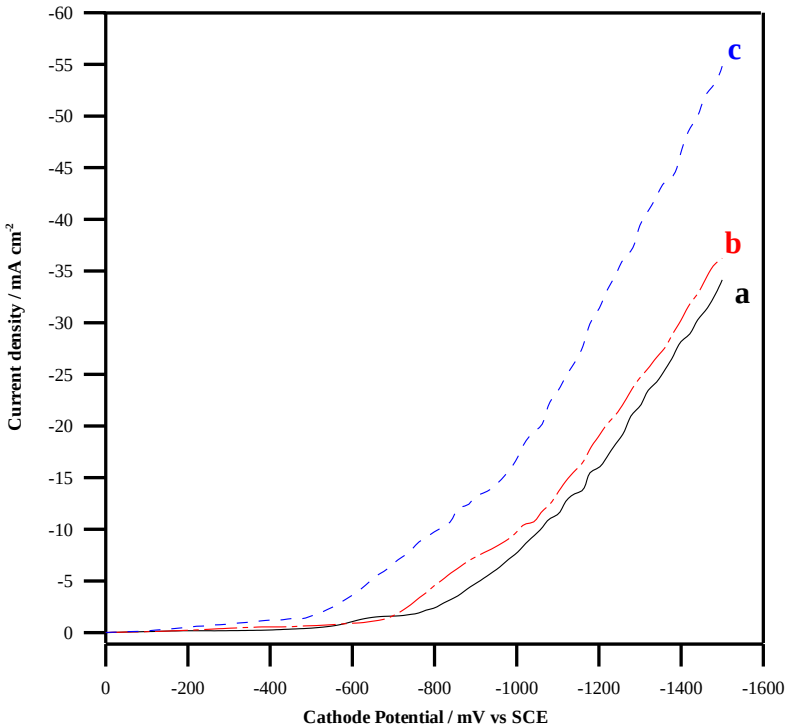

Figure 5. Cathodic polarization curves for the deposition of Ni-Co alloy on steel at different stirring speeds: (a) 0, (b) 600, and (c) 1500 rpm. Scan rate = 20 mV/s.

3.2. Ni-Co alloy composition and current efficacy

The current efficacy can be defined as the ratio between the actual mass of deposited metal to that which would have obtained if all the current had been used for deposition [42]. It depends not only on the applied current but also, on the other deposition variables, like electrolyte composition, pH, temperature, the existence of additives, deposition time, and agitation.

The CCE for metals and alloys is a significant factor for the electrodeposition process. It is a guide for the influential utilization of applied electrical energy [39]. The CCE of Ni-Co plating was established beneath various deposition parameters. In general, the total cathodic current efficacy of the Ni-Co alloy is great but does not attain 100 % due to the simultaneous discharge of hydrogen that results from water reduction [42, 43].

Two accepted mechanisms have been reported for hydrogen evolution reaction during the electrodeposition of the metals (M) alloys from aqueous solutions: (i) reduction (Eq. (11), followed by recombination (Eq. (12)) or (ii) reduction, followed by electrochemical desorption (Eq. (13)), [43, 44].

$$M + H_2O + e^- \rightarrow M{-}H_{ads} + OH^- \quad (11)$$

$$M{-}H_{ads} + M{-}H_{ads} \rightarrow 2M + H_2 \quad (12)$$

$$M{-}H_{ads} + H^+ + e^- \rightarrow M + H_2 \quad (13)$$

The cathodic current efficacy and the composition of Ni-Co alloy as a function of some deposition parameters were demonstrated in Figs. 6 – 10. According to the literature [16, 45, 46], the electrodeposition of Ni-Co alloy belongs to anomalous type, however, our results contradict this. According to our data, the percent of Co metal in the coating is often smaller than its percent in the bath. This behavior is characteristic of the plating from a regular or normal plating system [47].

For regular type, the nobler metal, Ni, should be reduced more easily than the less noble metal, Co, producing higher nickel content in the multilayers [48]. However, at certain deposition parameters, e.g., higher $[Ni^{2+}]$ / $[Co^{2+}]$ ratio (~ 8 to 20), the composition curve of Co metal located above the CRL. i.e., the deposition is changed from regular to anomalous type. It was reported that this is caused by some kinetic factors, which make nickel deposition over cobalt harder, and enable the deposition of cobalt over cobalt or nickel to happen faster and easily [48, 49].

Hydroxide suppression mechanism is a commonly passable explication for anomalous electrodeposition behavior. Due to the change of the pH value near the steel cathode as a result of hydrogen evolution, the metal hydroxide $Me(OH)_2$, or mono-hydroxide $Me(OH)^+$ is formed as intermediates during the alloy deposition [50, 51]. In the mechanism, the less noble metal mono-hydroxide, $Co(OH)^+$, which acts as a charge-transfer intermediate for the Co metal is preferably adsorbed at the cathode surface over that of the nobler one (Ni). As a result, an enriched film of $Co(OH)^+$ is formed on the cathode surface and inhibits the adsorption of $Ni(OH)^+$ by blocking its access to the cathode surface. Thus, the reduction of Co is promoted over that of Ni [49, 51]. Based on the considerations provided, the reaction pathway is assumed as follows [43, 44]:-

$$2H_2O + 2e^- \leftrightarrow H_2 + 2OH^- \quad (14)$$

$$Co^{2+} + OH^- \leftrightarrow Co(OH)^+ \quad (15)$$

$$Co(OH)^+_{(aq)} \leftrightarrow Co(OH)^+_{(ads)} \quad (16)$$

$$Co(OH)^+_{(ads)} + 2e^- \leftrightarrow Co + OH^- \quad (17)$$

Fig. (6) illustrates the effect of $[Ni^{2+}]$ / $[Co^{2+}]$ molar ratio on the percent of cobalt in the alloy and on the cathodic current efficacy. The data reveal that the Co % in the alloy diminishes with a rising $[Ni^{2+}]$ / $[Co^{2+}]$ molar ratio from 0.66 to 19. Increasing Ni^{2+} amount in the bath compensates for the lessening of Ni^{2+} ions in the cathodic diffusion layer. This supports the efficacy of Ni deposition at the expense of Co. The cathodic efficacy increases with $[Ni^{2+}]$ / $[Co^{2+}]$ molar ratio owing to an improvement in the efficacy of Ni plating [48].

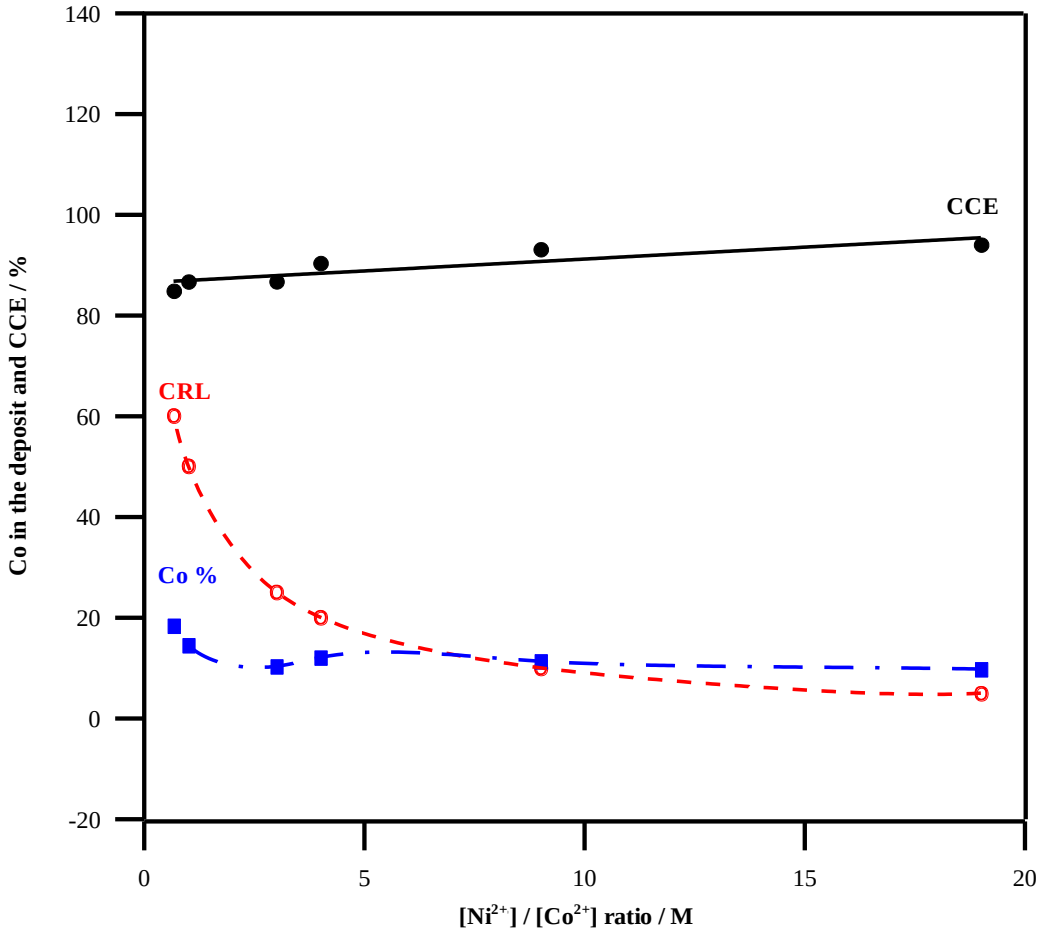

Figure 6. Effect of $[Ni^{2+}]/[Co^{2+}]$ molar ratio on the cathodic current efficacy (CCE) and the percent of Co in the deposit. The CRL represents the percentage of cobalt in the bath.

The curves of Fig. (7) reveal that the citrate concentration has no remarked effect on the quantity of cobalt in the alloy, which is nearly constant. Raising the citrate concentration from 0.3 to 1 M decreases the CCE because of an increase in the stability of different Ni-citrate complexes. Therefore, the reduction of the free Ni^{2+} ions is inhibited at the expense of the discharge of H^+ ions [48].

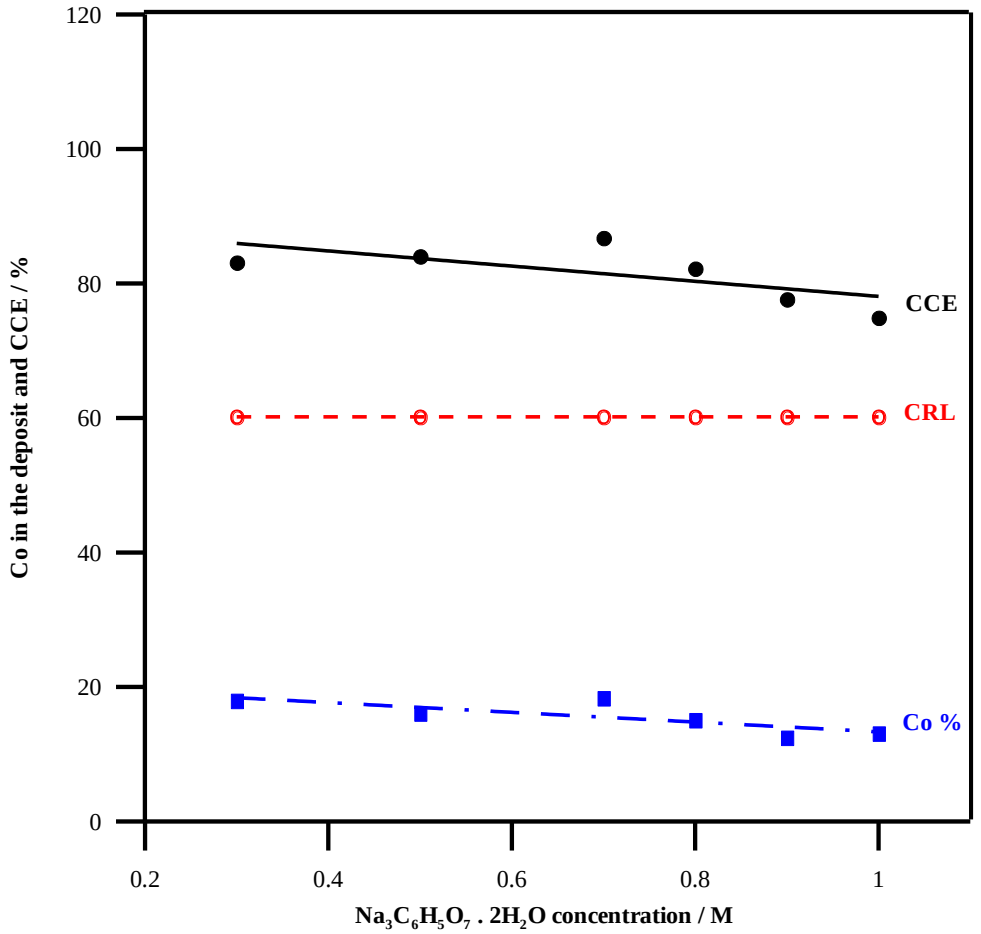

Figure 7. Effect of $Na_3C_6H_5O_7$. $2H_2O$ concentration on the cathodic current efficacy (CCE) and the percent of Co in the deposit. The CRL represents the percentage of cobalt in the bath.

Fig. (8) illustrates the impact of the deposition current on the alloy composition and on the current efficacy. Raising the applied current has no considerable impact on the Co % in the deposit, which is almost constant. An increase in the current density diminishes the CCE for the alloy plating. This is ascribed to a significant decrease in the efficacy of nickel deposition at the expense of hydrogen evolution. Another reason for the decreased metal deposition at elevated current densities can be assigned to the fact that the rate of transport of ions being insufficient to maintain the number of metal ions that arrive at the cathode surface from the bulk of the solution [52].

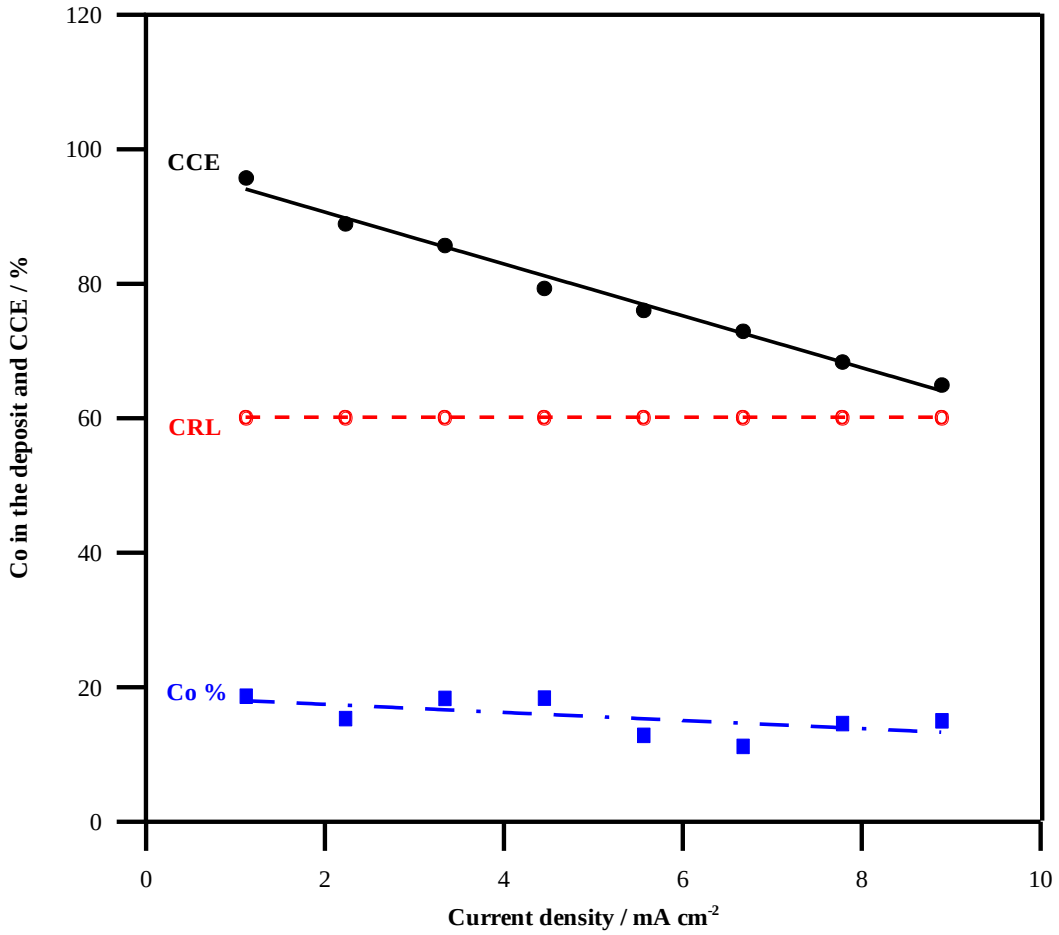

Figure 8. Effect of current density on the cathodic current efficacy (CCE) and the percent of Co in the deposit. The CRL represents the percentage of cobalt in the bath.

Plating temperature is the most important factor that affects the electrodeposition of alloys as it is straightway related to their composition and properties. The plating rate is also influenced by plating temperature as the transfer of ions from the electrolyte bulk to the cathode surface increases with temperature. The impact of temperature on the % of Co in the plating alloy and on the current efficacy was shown in Fig. (9). As the temperature increases, both the cobalt content and the current efficacy of alloy plating decrease. The impact of temperature on the deposited alloy composition is controlled by polarization and diffusion. At high temperatures, polarization increases the amount of Ni, the nobler metal, in the thin films. On the other hand, diffusion promotes the plating of Co, the active metal. Actually, it appears that the impact of diffusion is more pronounced than polarization and the Co % in the coatings ameliorates with temperature [16]. The decrease of CCE at high temperatures is ascribed to an increase in the rate of hydrogen ions discharge as anticipated from the polarization diagrams, Fig. (5). As a matter of fact, the alloy deposition may be diminished by diffusion inhibiting impact because of the evolution of hydrogen and the formation of bubbles [53].

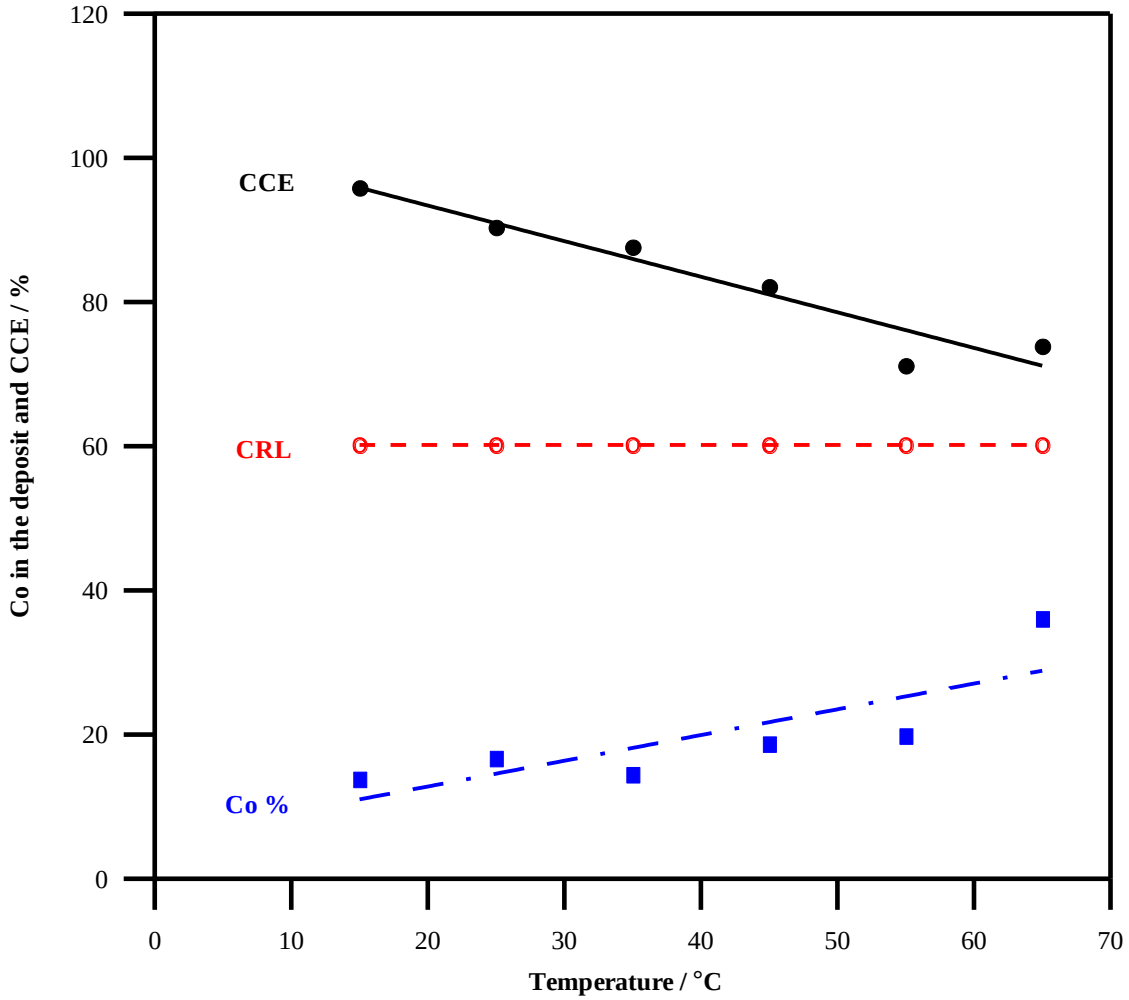

Figure 9. Effect of temperature on the cathodic current efficacy (CCE) and the percent of Co in the deposit. The CRL represents the percentage of cobalt in the bath.

The effect of bath agitation on the alloy composition and on the deposition efficacy is demonstrated in Fig. (10). The percentage of cobalt in the alloys extremely increases from 0.69 to 31.4 % by increasing the stirring speed of the plating solution from 0 to 1500 rpm. The CCE of alloy deposition also increases with increasing the stirring speed. Electrolyte agitation achieves electrolyte homogeneity and enhances mass transfer from the bulk electrolyte to the cathode surface [41].

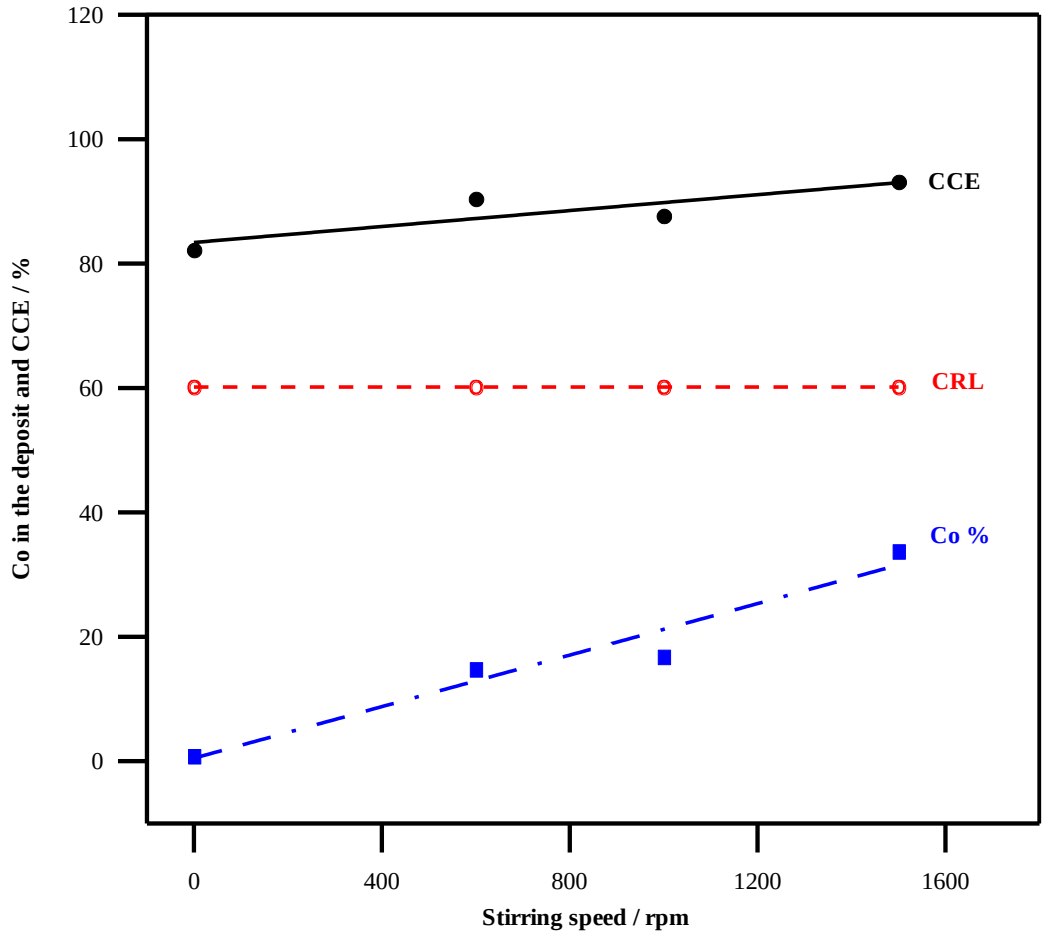

Figure 10. Effect of agitation speed on the cathodic current efficacy (CCE) and the percent of Co in the deposit. The CRL represents the percentage of cobalt in the bath.

3.3 Throwing power (TP) and throwing index (TI) measurements

The impacts of bath composition and different plating parameters on the TP of alkaline citrate baths for the electrodeposition of Ni-Co alloys were examined. The magnitudes of TP & TI are summarized in Table (2).

According to Table (2), it is shown that decreasing the $[Ni^{2+}]$ / $[Co^{2+}]$ ratio improves the magnitudes of TP &TI. Raising the citrate ion concentration in the plating bath enhances TP and TI because of diminishing the cathodic polarization. Otherwise, elevating the plating current density dramatically lessens the values of TP &TI due to hydrogen evolution. Along the same lines, increasing the deposition temperature to 55 °C decreases the TP and TI owing to a large lessen in the amount of the cathodic polarization.

There is no question that the alkaline citrate bath for Ni-Co alloy electroplating has a good throwing power and throwing index.

Table 2. Effect of bath composition, and plating variables on the throwing power and throwing index of Ni-Co alloy electroplating.

Bath composition				**Plating variables**			**T.I** (%)	**T.P** (%)
$[Ni^{2+}]$ / $[Co^{2+}]$ (M)	Sod. citrate (M)	Na_2SO_4 (M)	pH	c.d (mA cm^{-2})	Time (min.)	Temp. (^oC)		
19	0.3	0.3	10	3.33	20	25	1.41	15.55
0.66	0.3	0.3	10	3.33	20	25	2.17	40.91
0.66	1	0.3	10	3.33	20	25	2.68	51.35
0.66	0.3	0.3	10	1.11	20	25	5.02	91.30
0.66	0.3	0.3	10	8.88	20	25	1.82	30.77
0.66	0.3	0.3	10	1.11	20	55	2.40	38.46

3.4. Morphology and structure of the depositing alloy

Morphology is one of the most important properties of plated metals or alloys. Actually, it depends on the kinetic variables of the plating process. The deposition current density or overpotential affects the grain size, nucleation, and growth rate of the deposit [54].

The existence of complexes in the plating bath affects the equilibrium potentials of deposited metals, the amount of overvoltage, and the nature of deposits. For complex baths, the overpotential usually increases, the particle size of the coats diminishes, and the forming of dendritic deposits is restrained [16].

Generally, most of the Ni-Co alloy coatings obtained in this work have bright grey colors. They are all homogenous, regular, and compact with good adherence to the cathode surface. The brightness of the deposits is improved by increasing the Ni^{2+}ions and citrate amounts in the bath. On the contrary, the brightness gradually vanishes as the current density increases. Raising the bath temperature causes the forming of black deposits.

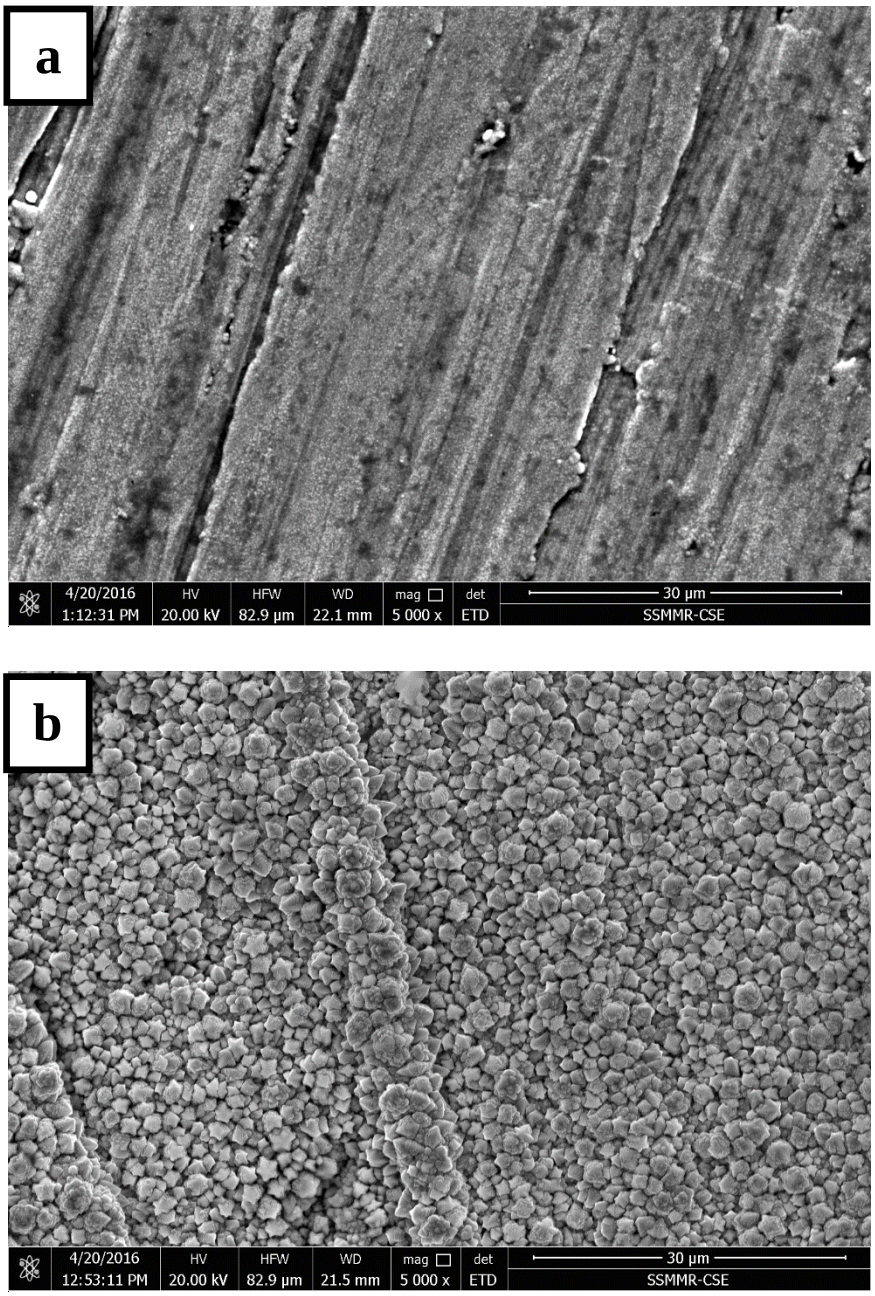

Figure 11. Scanning electron micrographs of electrodeposited Ni-Co alloy obtained under different current densities: (a) 1.11 and (b) 8.89 mA cm^{-2}.

Fig. (11) presents the impact of current density on the morphology of plated Ni-Co alloy. The deposits (Ni_{81} Co_{19}) obtained at a small current density (1.11 mA cm^{-2}) are compact, leveled, and smooth with a small grain size, Fig. (11a). This morphology arises because the rate of nucleation exceeds the growth rate. Raising the applied current density to 8.88 mA cm^{-2} causes the formation of dense and polyhedral deposits (Ni_{85} Co_{15}). It is worth observing that the coating has a cauliflower-like structure, Fig. (11b).

The photos of Fig. (12) demonstrate the impact of temperature on the appearance of plated Ni-Co alloy. Low temperature (15 °C) encourages the formation of smooth and compact deposits

(Ni_{86} Co_{14}) with fine grain size, Fig. (12a). The deposit contains some pores due to the evolution of hydrogen bubbles. An elevated temperature leads to the formalization of granular compact deposits (Ni_{64} Co_{36}), Fig. (12b).

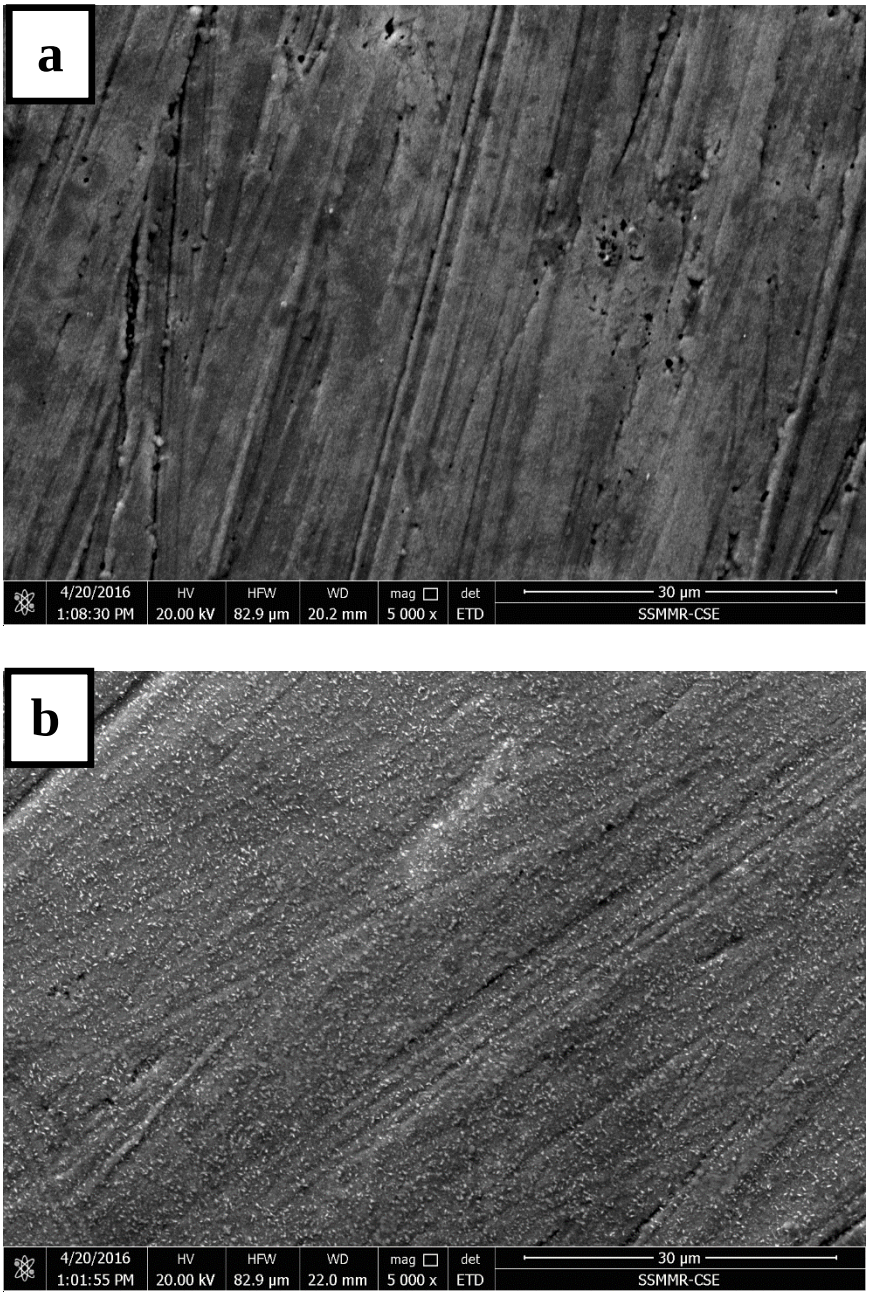

Figure 12. Scanning electron micrographs of electrodeposited Ni-Co alloy obtained under different temperatures: (a) 15 and (b) 65 ˚C.

The phase and structure of Ni-Co alloys plated from selected baths under various practical conditions were tested by the X-ray diffraction technique. The examination by X-ray illustrates that whatever the composition of the tub and deposition parameters, the whole deposits are well-crystalline. The XRD spectra confirmed that the structure of the deposited Ni-Co alloys is a single solid solution

with an (FCC) lattice structure [55]. This is confirmed by the absence of the Co peaks phase in the spectra. The crystal lattice of Ni matrix may be partly substituted by Co, as the microstructure of Ni and Co is resembles and a solid solution is formed [3]. The plated alloys exhibit 3 well-defined peaks at 44.5°, 51.8°, and 76.4°. The peaks are ascribed to (111), (200), and (220) growth planes, respectively [45].

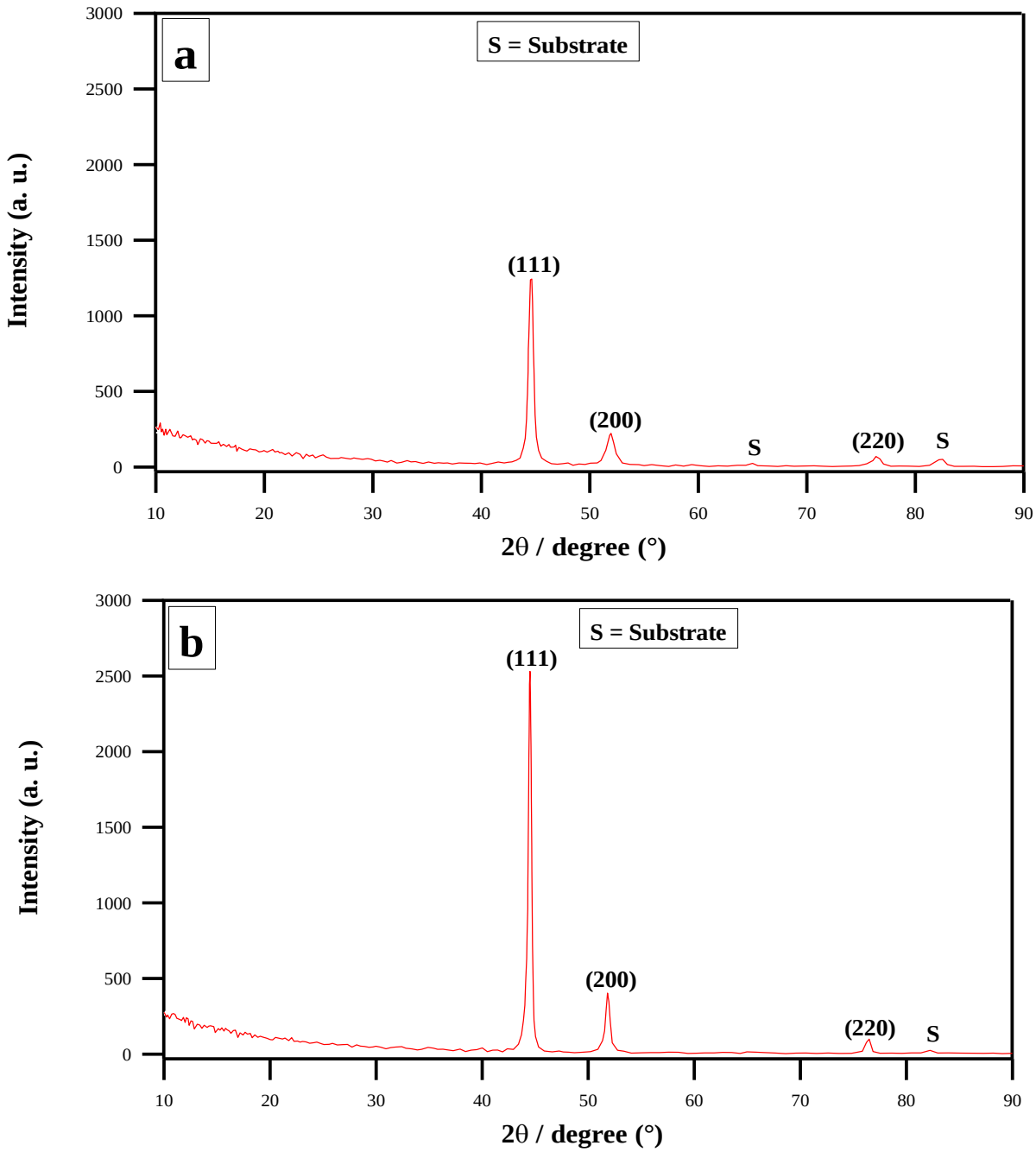

Figure 13. X-ray diffraction patterns of electrodeposited Ni-Co alloy obtained under different current densities: (a) 1.11 and (b) 8.89 mA cm^{-2}

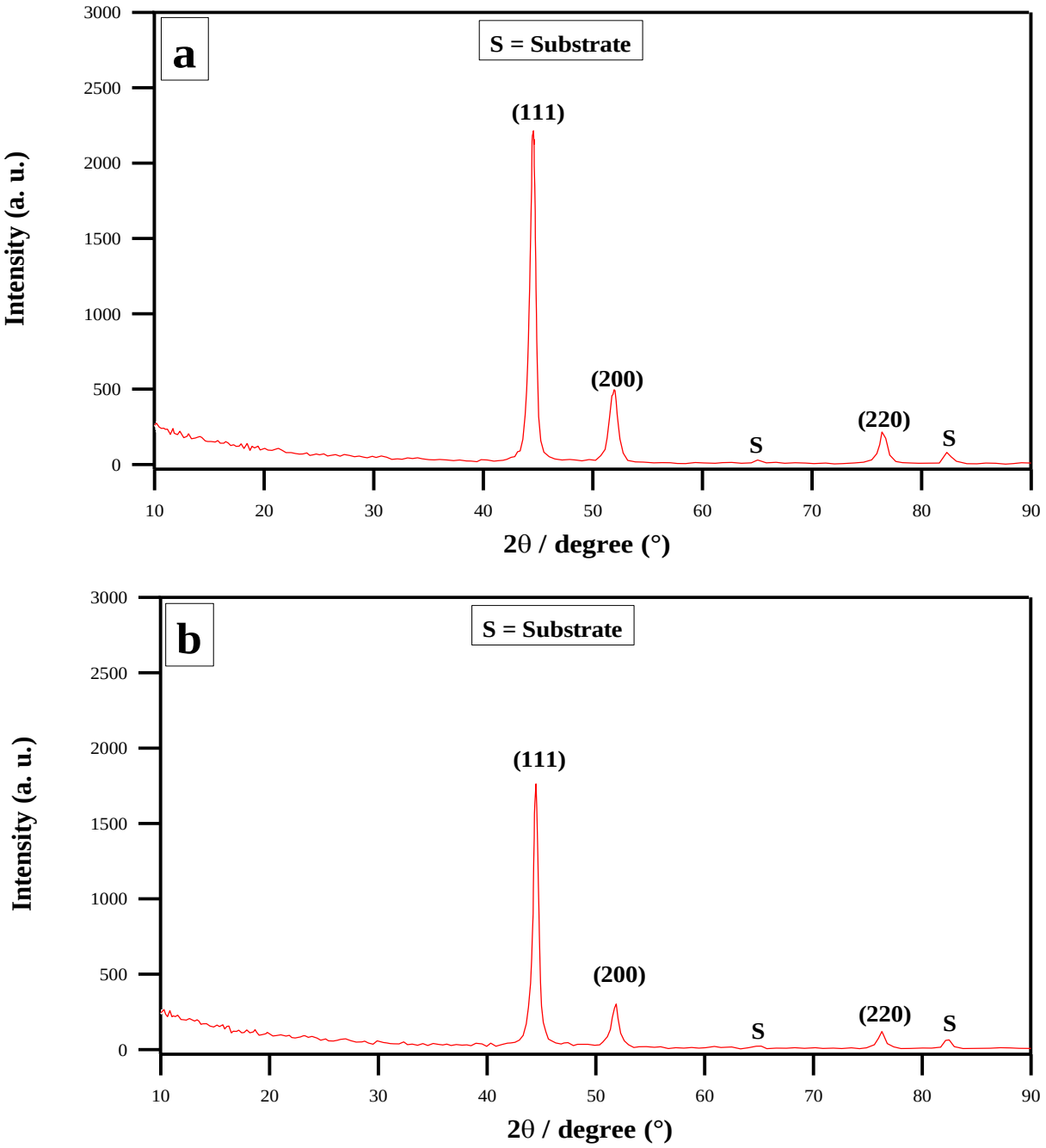

Figure 14. X-ray diffraction patterns of electrodeposited Ni-Co alloy obtained under different temperatures: (a) 15 and (b) 65 ˚C.

The diffraction planes are acute and well-defined, referring to good crystallization. The intensity of the (111) peak is the highest (relative intensity = 100 %), indicating that the plated Ni-Co alloys show the preferred orientation of (111), Figs. (13) and (14). The impact of current density on XRD patterns of plated Ni-Co alloy is presented in Fig. (13). The plane (111) is the major one over the examined current density limit. The crystallinity of the deposits is ameliorated by increasing the current density. In addition, the intenseness of the planes (111), and (200) increases with current density, Fig. (13 b).

Fig. (14) shows the impact of bath temperature on the crystallinity of plated Ni-Co alloy. The diffraction plane (111) is the most intense one over the entire examined temperature limit. Raising the temperature to 65 °C decreases the intenseness of the planes (111), (200), and (220), Fig. (14 b).

4. CONCLUSIONS

- The electrochemical deposition of Ni-Co alloy thin films onto steel coupons was investigated from solutions containing citrate ions under various operating conditions.
- The plating process was established from a bath containing $NiSO_4.6H_2O$, $CoSO_4.7H_2O$, $Na_3C_6H_5O_7.2H_2O$, and Na_2SO_4.
- Increasing the concentration of citrate ion in the plating solution moves the plating potential to highly negative values.
- The total cathodic current efficacy for Ni-Co alloy deposition is great but less than 100 % due to the evolution of hydrogen bubbles.
- The deposition of Ni-Co alloy pertains to the regular category.
- The composition curves of the Co metal exist below the composition reference line (CRL).
- The alkaline citrate bath for Ni-Co electroplating has good throwing power.
- The Ni-Co alloy plates obtained are bright with a grey color.
- The XRD spectra confirmed that the structure of the electrodeposited Ni-Co alloys is a single solid solution with an (FCC) lattice structure.

ACKNOWLEDGMENTS
Taif University Researchers Supporting Project number (TURSP – 2020/136), Taif University, Taif, Saudi Arabia.

References

1. L. Shi, C. Sun, P. Gao, F. Zhou, W. Liu, *Appl. Surf. Sci*., 252 (2006) 3591–3599.
2. B. Bahadormanesh, A. Dolati, M. R. Ahmadi, *J. Alloys Compd*., 509 (2011) 9406– 9412.
3. L. Tian, J. Xu, S. Xiao, Vacuum, 86 (2011) 27–33.
4. Sh. Hassani, K. Raeissi, M. Azzi, D. Li, M. A. Golozar, J. A. Szpunar, *Corros. Sci.*, 51 (2009) 2371–2379.
5. C. Ma, S. C. Wang, L. P. Wang, F. C. Walsh, R. J. K. Wood, *Wear*, 306 (1–2) (2013) 296–303.
6. F. J. Pérez–Alonso, C. Adán, S. Rojas, M. A. Peña, J. L. G. Fierro, *Int. J. Hydrogen Energy*, 40 (1) (2015) 51–61.
7. C. Lupi, A. Dell'Era, M. Pasquali, *Int. J. Hydrogen Energy*, 34 (2009) 2101–2106.
8. M. Srivastava, V. E. Selvi, V. K. W. Grips, K. S. Rajam, *Surf. Coat. Technol.*, 201 (6) (2006) 3051–3060.
9. A. Karpuz, H. Kockar, M. Alper, O. Karaagac, M. Haciismailoglu, *Appl. Surf. Sci.*, 258 (2012) 4005–4010.

10. S. Olvera, E. M. Arce Estrada, J. Sanchez–Marcos, F. J. Palomares, L. Vazquez, P. Herrasti, *Mater. Charact.*, 105 (2015) 136–143.
11. O. Ergeneman, K. M. Sivaraman, S. Pané, E. Pellicer, A. Teleki, A. M. Hirt, M. D. Baró, B. J. Nelson, *Electrochim. Acta*, 56 (3) (2011) 1399–1408.
12. K. M. Cole, D.W. Kirk, S. J. Thorpe, *J. Electrochem. Soc.,* 165 (2018) J3122–J3129.
13. D.Y. Park, K.S Park, J. M. Ko, D.H. Cho, S. H. Lim, W.Y. Kim, B.Y. Yoo, N.V. Myung, *J. Electrochem. Soc.*, 153 (2006) C814–C821.
14. L. Yi-Jae, J. Yeong Park, *Appl. Surf. Sci.*, 277 (2013) 100 – 104.
15. A.M.P. Sakita, E.C. Passamani, H. Kumar, D.R. Cornejo, C.S. Fugivara, R.D. Noce, A.V. Benedetti, *Mater. Chem. Phys.,* 141 (2013) 576 – 581.
16. M. M. Kamel, *J. Appl Electrochem.,* 37 (2007) 483–489.
17. S.M. Rashwan, A.E. Mohamed, S.M. Abd El-Wahaab, M.M. Kamel, *J. Appl. Electrochem.*, 33 (2003) 1035-1042.
18. N. S. Mbugua, M. Kang, Y. Zhang, N. J. Nadiithi, G. V. Bertand, L. Yao, *Mater.,* 13 (2020) 3475 – 3505.
19. Y. E. Sknar, I. V. Sknar, O. O. Savchuk, F. I. Danilov, *Surf. Coat. Technol.*, 387 (2020) 125542.
20. Y. Jiang, C. Y. Chen, T. F. M. Chang, X. Luo, D. Yamane, M. Sone, *Electrochem.*, 2 (2021)1-9.
21. I. M. A. Omar, K. M. Emran, M. Aziz, *Int. J. Electrochem.*, 16 (2021) 1-20.
22. M. S. Safavi, A. Rasooli, F. A. Sorkhabi, *Trans. Inst. Met. Finish.*, 98 (6) (2020) 320–327.
23. A. Karimzadeh, M. Aliofkhazraei, F. C. Walsh, *Surf. Coat. Technol.*, 372 (2019) 463–498.
24. G. R. Wang, P. S. Hung, S.Y. Chang, J. M. Yang, Y. C. Tseng, P. W. Wu, *J. Electrochem. Soc.*, 167 (2020) 022505.
25. R. M. Al Radadi, M. A. M. Ibrahim, *Korean J. Chem. Eng.*, 37 (9) (2020) 1599 – 1608.
26. J. Wang, H. Shao, S. Ren, A. Hu, M. Li, *Appl. Surf. Sci.*, 539 (2021) 148045.
27. X. Qiao, H. Li, W. Zhao, D. Li, *Electrochim. Acta*, 89 (2013) 771–777.
28. S. S. Abd El Rehim, S. M. Abd El Wahaab, M. A. M. Ibrahim, M. M. Dankeria, *J. Chem Technol. Biotechnol.*, 73 (1998) 369–376.
29. Alina–Crina Ciubotariu, L. Benea, M. Lakatos–Varsanyi, V. Dragan, *Electrochim. Acta*, 53 (2008) 4557–4563.
30. M. M. Kamel, Z. M. Anwer, I. T. Abdel–Salam, I. S. Ibrahim, *Trans. Inst. Met. Finish.*, 88 (4) (2010) 191–197.
31. M. M. Kamel, Z. M. Anwer, I. T. Abdel–Salam, I. S. Ibrahim, *Surf. Interface Anal.*, 46 (2014) 442–448.
32. J. Aikaitė, O. Gylienė, O. Nivinkienė, Institute of Chemistry, *A. Goštauto 9 LT–2600 Vilnius*, Lithuania, (2003), 135–139.
33. Ed. D. D. Perrin, L. G. Sillen, Stability constants of metal–ion complexes. Part B: Organic Ligands, Pergamon Press; Oxford, (1979).
34. A. Deepatana, M. Valix, Adsorption of metals from metal-organic complexes derived from bioleaching of nickel laterite ores, Engineering Conferences International (2004).
35. L. C. Qun, L. X. Hai, W. Z. Xin, G. H. Jun, *Trans. Nonferrous Met. Soc. China*, 17 (2007) 1300–1306.
36. L. Trinta de Farias, A. S. Luna, D. C. Baptista do Lago, L. Ferreira de Senna, *Mater. Res.*, 11 (1) (2008) 1–9.
37. S. S. Abd El Rehim, S. M. Abd El Wahaab, S. M. Rashwan, Z. M. Anwar, *Trans. Inst. Met. Finish.*, 77 (6) (1999) 242–245.
38. S. S. Abd El Rehim, S.M. Abd El Wahaab, S. M. Rashwan, Z. M. Anwar, *J. Chem. Technol. Biotechnol.*, 77 (2000) 1–8.
39. J. Vazquez–Arenas, L. Altamirano–Garcia, T. Treeratanaphitak, M. Pritzker, R. Luna–Sanchez, R. Cabrera–Sierra, *Electrochim. Acta*, 65 (2012) 234–243.
40. M. A. M. Ibrahim, R. S. Bakdash, *Surf. Coat. Technol.*, 282 (2015) 139–148.

41. B. Bakhit, A Akbari, *J. Alloys Compd.*, 560 (2013) 92–104.
42. R. K. Saha, T. I. Khan, *Surf. Coat. Technol.*, 205 (2010) 890–895.
43. R. Oriňáková, A. Oriňák, G. Vering, I. Talian, R. M. Smith, H. F. Arlinghaus, *Thin Solid Films*, 516 (2008) 3045–3050.
44. H. Cesiulis, A. Budreika, *Mater. Sci.*, 16 (1) (2010) 52–57.
45. Y. H. You, C. D. Gu, X. L. Wang, J. P. Tu, *Surf. Coat. Technol.*, 206 (2012) 3632–3638.
46. L.L. Tian, J.C. Xu, C.W. Qiang, *Appl. Surf. Sci.*, 257 (2011) 4689 - 4694.
47. A. Brenner, Electrodeposition of Alloys. Principles and Practice, vols. 1 and 2, Academic Press, New York, 1963.
48. S. M. S. I. Dulal, E. A. Charles, *J. Alloys Compd.*, 455 (2008) 274–279.
49. J. Vazquez–Arenas, T. Treeratanaphitak, M. Pritzker, *Electrochim. Acta*, 62 (2012) 63–72.
50. K. Vathsala, T. V. Venkatesha, *Appl. Surf. Sci.*, 257 (2011) 8929–8936.
51. Paulo C. Tulio, Stanley E. B. Rodrigues, Ivani A. Carlos, *Surf. Coat. Technol.*, 202 (2007) 91–99.
52. D. K. Singh, V. B. Singh, *Mater. Sci. Eng.*, A, 532 (2012) 493–499.
53. R. Y. Ying, P. K. Ng, *J. Electrochem. Soc.*, 135 (1988) 2464.
54. N. D. Nikolić, Lj. J. Pavlović, M. G. Pavlović, K. I. Popov, *Electrochim. Acta*, 52 (2007) 8096–8104.
55. B. Bakhit, A. Akbari, F. Nasirpouri, M. G. Hosseini, *Appl. Surf. Sci.*, 307 (2014) 351–359.

© 2021 The Authors. Published by ESG (www.electrochemsci.org). This article is an open-access article distributed under the terms and conditions of the Creative Commons Attribution license (http://creativecommons.org/licenses/by/4.0/).